



A Massive-born Neutron Star with a Massive White Dwarf Companion

Ismaël Cognard, Paulo C C Freire, Lucas Guillemot, Gilles Theureau, Thomas M Tauris, Norbert Wex, Eleni Graikou, Michael Kramer, Benjamin Stappers, Andrew G Lyne, et al.

► To cite this version:

Ismaël Cognard, Paulo C C Freire, Lucas Guillemot, Gilles Theureau, Thomas M Tauris, et al.. A Massive-born Neutron Star with a Massive White Dwarf Companion. The Astrophysical Journal, 2017, 844 (2), 13 p. 10.3847/1538-4357/aa7bee . insu-01670513

HAL Id: insu-01670513

<https://insu.hal.science/insu-01670513>

Submitted on 21 Dec 2017

HAL is a multi-disciplinary open access archive for the deposit and dissemination of scientific research documents, whether they are published or not. The documents may come from teaching and research institutions in France or abroad, or from public or private research centers.

L'archive ouverte pluridisciplinaire **HAL**, est destinée au dépôt et à la diffusion de documents scientifiques de niveau recherche, publiés ou non, émanant des établissements d'enseignement et de recherche français ou étrangers, des laboratoires publics ou privés.

A MASSIVE-BORN NEUTRON STAR WITH A MASSIVE WHITE DWARF COMPANION

ISMAËL COGNARD,^{1,2} PAULO C. C. FREIRE,^{3,2} LUCAS GUILLEMOT,^{1,2} GILLES THEUREAU,^{1,2,4} THOMAS M. TAURIS,^{3,5}
NORBERT WEX,³ ELENİ GRAIKOU,³ MICHAEL KRAMER,³ BENJAMIN STAPPERS,⁶ ANDREW G. LYNE,⁶ CEES BASSA,⁷
GREGORY DESVIGNES,³ AND PATRICK LAZARUS³

¹*Laboratoire de Physique et Chimie de l'Environnement et de l'Espace, Université d'Orléans/CNRS, F-45071 Orléans Cedex 02, France*

²*Station de radioastronomie de Nançay, Observatoire de Paris, CNRS/INSU, F-18330 Nançay, France*

³*Max-Planck-Institut für Radioastronomie, Auf dem Hügel 69, D-53121 Bonn, Germany*

⁴*LUTH, Observatoire de Paris, PSL Research University, CNRS, Université Paris Diderot, Sorbonne Paris Cité, F-92195 Meudon, France*

⁵*Argelander-Institut für Astronomie, Universität Bonn, Auf dem Hügel 71, D-53121 Bonn, Germany*

⁶*Jodrell Bank Center for Astrophysics, School of Physics and Astronomy, The University of Manchester, M13 9PL, UK*

⁷*ASTRON, The Netherlands Institute for Radioastronomy, Postbus 2, 7900 AA, Dwingeloo, The Netherlands*

ABSTRACT

We report on the results of a 4-year timing campaign of PSR J2222–0137, a 2.44-day binary pulsar with a massive white dwarf (WD) companion, with the Nançay, Effelsberg and Lovell radio telescopes. Using the Shapiro delay for this system, we find a pulsar mass $m_p = 1.76 \pm 0.06 M_\odot$ and a WD mass $m_c = 1.293 \pm 0.025 M_\odot$. We also measure the rate of advance of periastron for this system, which is marginally consistent with the GR prediction for these masses. The short lifetime of the massive WD progenitor star led to a rapid X-ray binary phase with little ($< 10^{-2} M_\odot$) mass accretion onto the neutron star (NS); hence, the current pulsar mass is, within uncertainties, its birth mass, which is the largest measured to date. We discuss the discrepancy with previous mass measurements for this system; we conclude that the measurements presented here are likely to be more accurate. Finally, we highlight the usefulness of this system for testing alternative theories of gravity by tightly constraining the presence of dipolar radiation. This is of particular importance for certain aspects of strong-field gravity, like spontaneous scalarization, since the mass of PSR J2222–0137 puts that system into a poorly tested parameter range.

Keywords: pulsars: general — pulsars: individual J2222–0137 — stars: neutron star — white dwarfs — binaries: close — X-rays: binaries

1. INTRODUCTION

1.1. The PSR J2222–0137 binary system

PSR J2222–0137 is a recycled pulsar ($P = 32.8$ ms, $B = 0.76 \times 10^9$ G) discovered in the Green Bank Telescope (GBT) 350 MHz drift scan survey (Boyles et al. 2013). It is in a binary system with orbital period $P_b = 2.44576$ d, the projected semi-major axis of the pulsar’s orbit is $x = 10.848$ light seconds (lt-s).

This results in a mass function of $0.229 M_\odot$, which implies a relatively massive companion: in a follow-up paper, Kaplan et al. (2014, henceforth Paper I) estimated the masses of the components of the system to be $m_p = 1.20 \pm 0.14 M_\odot$ for the pulsar, $m_c = 1.05 \pm 0.06 M_\odot$ for the companion and an orbital inclination of $i = 86.8 \pm 0.04^\circ$ (or $i' = 180^\circ - i = 93.2 \pm 0.04^\circ$), from the Shapiro delay in this system. As discussed in Paper I, the orbital eccentricity of the system ($e = 0.00038$) implies that the companion is a white dwarf (WD) star: the formation of a second neutron star (NS) would have induced an orbital eccentricity (from kicks and, even in the case of a symmetric explosion, from the sudden loss of the binding energy of the NS) at least two orders of magnitude larger, with no possibility of subsequent tidal circularization of the orbit. The system can therefore be classified as an intermediate mass binary pulsar (IMBP, see Camilo 1996; Tauris et al. 2012). Although small, the reported pulsar mass was not considered surprising as it is similar to that of another IMBP, PSR J1802–2124, with $m_p = 1.24 \pm 0.11 M_\odot$ and $m_c = 0.78 \pm 0.04 M_\odot$ (Ferdman et al. 2010).

PSR J2222–0137 has a dispersion measure (DM) of only $3.28 \text{ cm}^{-3} \text{ pc}$, one of the lowest for any pulsar. According to the NE2001 model (Cordes & Lazio 2002) of the electron distribution in the Galaxy, this implies a distance of 312 pc. This motivated a Very Long Baseline Interferometry (VLBI) astrometric campaign that obtained the most precise VLBI distance for any pulsar, $d = 267.3^{+1.2}_{-0.9}$ pc (Deller et al. 2013, henceforth Paper II); 15 % smaller than the NE2001 prediction. They also measured unusually precise values for the position and proper motion of the system: the total proper motion is large ($\mu_T = 45.09(2) \text{ mas yr}^{-1}$), but the implied transverse velocity ($v_T = 57.1^{+0.3}_{-0.2} \text{ km s}^{-1}$ in the Barycentric reference frame) is typical among recycled pulsar systems (e.g., Gonzalez et al. 2011). Because of the relatively large size of the pulsar orbit and the proximity of the system, Deller et al. (2013) were able to detect, for the first time, the orbital motion of the pulsar in the astrometric data; from this they derived a position angle (PA) of the line of nodes, $\Omega = 5^{+15}_{-20}^\circ$.

The relatively small distance to this binary pulsar allowed detailed multi-wavelength follow-up. Kaplan et al. (2014) observed the astrometric position of PSR J2222–0137 at optical wavelengths with the Keck I and II telescopes, and surprisingly the WD companion was not detected; this implies

that it is at least 100 times fainter than any other WD companion to a pulsar detected to date. Whether this is surprising or not depends on the temperature and radius of this WD. Assuming a WD mass of $1.05 M_\odot$, a WD radius of about 0.8 Earth radii (R_\oplus) was derived in Paper I. For this radius, the optical non-detection implies a surface temperature smaller than 3000 K. According to the WD cooling models of Bergeron et al. (2011) such a low temperature is only reached after the rapid cooling phase sets in following crystallization of the core, and the estimated cooling age is about 8 to 10 Gyr. The characteristic age of the pulsar is about 30 Gyr, which implies that an age of 8 - 10 Gyr cannot be excluded from spin considerations¹.

1.2. Motivation and outline of this work

We report on the results of a 4-year timing campaign of this pulsar with the Nançay (NRT), Effelsberg and Lovell radio telescopes. The motivation is to obtain more precise physical parameters for this system, in particular the mass of PSR J2222–0137, but also the mass of its WD companion.

The short stellar lifetime of the massive WD progenitor led to a rapid X-ray binary phase resulting, as discussed below, in little mass accretion onto the pulsar. Therefore, its current mass must be very similar to its birth mass. This contrasts with the evolution of the fastest-spinning pulsars which generally have much lower-mass companions; in those cases the long accretion phases that spun them up could in principle have substantially increased the NS mass.

Precise NS birth masses are important because they probe the final stellar evolution phases of massive stars as well as supernova explosion physics (Özel et al. 2012). Most NS birth masses (and certainly the most precise among them) have been measured in double neutron star systems (DNSs). Until 2013 all NSs in DNS systems had masses between 1.23 and $1.44 M_\odot$; this situation changed with the discovery of PSR J0453+1559 (Deneva et al. 2013): for this system $m_p = 1.559 \pm 0.005 M_\odot$ and $m_c = 1.174 \pm 0.004 M_\odot$ (Martinez et al. 2015). This implies that NSs are born with a wider range of masses than previously thought. This highlights the importance of increasing the sample of NS birth masses: we still don’t know how wide the distribution is and what the maximum is, and whether it is a single distribution, bimodal or more complex (Özel & Freire 2016; Antoniadis et al. 2017). Furthermore, increasing the (very small) sample of NS birth masses in systems with massive WD companions has the added benefit of verifying whether the companion mass and evolution have any effect on this distribution.

¹ Although the characteristic age does not provide a reliable age estimate for a recycled pulsar (Tauris et al. 2012), it represents an approximate upper limit for that age, assuming a braking index of 3. Therefore, if the characteristic age of PSR J2222–0137 were much smaller than 8 Gyr, we would be able to exclude the extreme age suggested by the cooling timescale.

The mass measurements in Paper I do not usefully place PSR J2222–0137 within the observed NS birth mass range: within 2σ , its mass is consistent with 0.92 and $1.48 M_{\odot}$. This motivated the long-term timing reported here that has yielded improved (and significantly larger) masses mainly by improving the measurement of the Shapiro delay and separating it from the rate of advance of periastron.

The remainder of the paper is structured as follows. In Section 2 we describe the details of the observations, data processing, and present two timing solutions for the pulsar with a description of how they were derived; one with positional fitting, the other using the previously derived VLBI position. The reasons for this are discussed in Section 3, where we make a detailed comparison of the astrometry derived from the timing with the VLBI astrometry. In Section 4 we present further timing results: an improved measurement of the Shapiro delay (we discuss the resultant component masses), a highly significant measurement of the rate of advance of periastron $\dot{\omega}$ and finally discuss the kinematic effects on the timing parameters. In Section 5, we discuss the measurement of the variation of the orbital period (\dot{P}_b) and the resulting limits on the emission of dipolar gravitational waves, we also discuss how precise this system might become with future timing. In Section 6, we discuss the past history of this system in light of the new mass measurements. Finally, in Section 7, we summarize our findings and discuss the prospects for continued timing of this system.

2. OBSERVATIONS AND DATA PROCESSING

Our observations of PSR J2222–0137 are summarized in Table 1. The pulsar has been observed regularly with the “low” (1.2 – 1.7 GHz, or “L band”) and “high” (1.7 – 3.0 GHz, or “S band”) receivers of the NRT for the ~ 1 hour the pulsar stays near transit since 2012 September 21; the last observation used in this work was on 2016 July 5. We used the Nançay Ultimate Pulsar Processing Instrument (NUPPI), a back-end similar to the Green Bank Ultimate Pulsar Processing Instrument (GUPPI) at the GBT² to process the signal which allows for real-time coherent dedispersion and folding of a bandwidth $BW = 512$ MHz (Liu et al. 2014). We note that the NUPPI data analyses presented in Liu et al. (2014) were affected by a lack of precision while reading crucial internal MJD dates by the PSRCHIVE (Hotan et al. 2004; van Straten et al. 2012) software, causing reduced timing precision. This issue has now been fixed and the corrected software has been extensively tested using NUPPI datasets.

From 2015 October 26 to November 28, and again between 2017 January 5 to 13, we conducted two intensive campaigns with the Effelsberg 100-m radio telescope, with the aim of confirming (and possibly improving) the Shapiro delay mea-

surements. Those data were taken with the 20-cm receiver (with $BW = 150$ MHz) and the central beam of the 7-beam system ($BW = 250$ MHz) using PSRIX (Lazarus et al. 2016) as a back-end. All observing data is presented in Table 1.

Observations of PSR J2222–0137 were made with the 76-m Lovell Telescope at Jodrell Bank using a 400-MHz total bandwidth, starting 2012 November 20 until 2016 June 4. The 400-MHz band was centred on 1532 MHz and was analysed using roach-based coherent dedispersion processing across five 80-MHz sub-bands. Each observation had a duration of between six and twenty-five minutes.

2.1. Polarimetry

In Figure 1, we display (in the inset, top panel) the pulse profile for PSR J2222–0137. This was obtained from the addition of the best Effelsberg detections of the pulsar, which were cleaned of RFI and then calibrated using the noise diode observations made every hour during the observations. This was done using the “PAC” program, which is part of PSRCHIVE using the “Single Axis” model. We corrected for the Faraday rotation of the pulsar using the rotation measure published in Paper I ($RM = 2.6(1) \text{ rad m}^{-2}$).

In the bottom panel of the inset, we display the PA of the linear polarization as a function of spin phase. This is measured in a counter-clockwise sense, starting from North through East. Furthermore, a system with an orbital inclination of zero degrees has its angular momentum pointing towards the Earth. This is the “observer’s convention” defined in Edwards et al. (2006) that is assumed in PSRCHIVE.

To this observed PA curve, we have tried to fit a rotating vector model (RVM, Radhakrishnan & Cooke 1969). This is not a clean fit: the PA profile is clearly more complex than described by a simple RVM model, so the interpretation is not straightforward. This is a situation that has been long observed among MSPs (e.g., Xilouris et al. 1998).

In order to obtain a meaningful model, we chose two longitude ranges (highlighted in black, ignored regions in gray), which avoid a pulse region that can be associated with so-called “core” emission, which is known to commonly disturb a smooth PA swing (Rankin 1983). This allows RVM fits to determine a viewing angle (ζ , the angle between the spin axis and the magnetic axis) that is similar to the orbital inclination of the system, i . This is expected given the fact that this pulsar is recycled: it was spun up with gas from its companion, this implies that there was a transfer of orbital angular momentum to the pulsar. This implies that after accretion the pulsar’s spin angular momentum was parallel to the orbital angular momentum. We see no signs of a disruptive event (like a second SN) that might have changed the orbital plane after the recycling episode, so the spin angular momentum should still be closely aligned with the orbital angular momentum.

² <http://safe.nrao.edu/wiki/bin/view/CICADA/GUPPISupportGuide>

Table 1. Observations of J2222–0137 and data reduction parameters

Telescope	Nançay L	Nançay S	Effelsberg	Lovell
Start of observations (MJD)	56191	56204	57321	56251
End of observations (MJD)	57527	57574	57766	57543
Bandwidth (MHz)	512	512	150/250	400
Bandwidth per TOA (MHz)	128	128	150/125	80
Center frequency (MHz)	1484	2539	1360	1532
Number of TOAs used in solution	1601	80	939	258
Time per TOA (s)	600	600	600	600
Weighted residual rms (μ s)	4.1	7.3	2.5	8.2
EFAC	1.0	1.0	1.0	1.0
EQUAD (μ s)	2.46	0.0	0.96	4.46

In the main panel, we display, for each value of magnetic inclination angle (α , the angle between the spin axis and the magnetic axis) and viewing angle ζ the quality of the RVM fit to the PA curve. At each point we keep α and ζ fixed, while minimizing the χ^2 -value in a least-squares fit to the reference phase ϕ_0 and reference PA ψ_0 . The inclined contour lines indicate the $1-\sigma$ region. Clearly, there is a strong correlation between α and ζ , which is a well known effect for a small pulse duty cycle as observed here (e.g. [Lorimer & Kramer 2004](#)).

In order to constrain the geometry further, we mark the constraint on the orbital inclination angle ($\zeta = i = 85.27^\circ$), which is derived from the Shapiro delay and the measurement of \dot{x} (see section 4), as an horizontal strip. This is the aforementioned constraint that the spin angular momentum of the pulsar is parallel to the orbital angular momentum.

Assuming a filled emission beam, we derive a distribution of magnetic inclination angles (lower panel) that is consistent with the observed pulse width. The vertical dashed lines indicate a $\pm 12^\circ$ region around 90° . As we can see, the region given by the intersection of the area allowed by the polarimetry and the measurement of the orbital inclination is well within the allowed region of magnetic inclination angles; this self-consistency suggests that the choice of longitude ranges we have made and the best-resulting RVM fit (Also displayed in the bottom panel of the inset, superposed to the measurements of the linear PA) is not entirely arbitrary, providing a reasonable estimate of $\alpha \sim 83^\circ$. This means that the magnetic pole passes only within a couple of degrees of the line of sight.

2.2. Data reduction for pulsar timing

All dedispersed pulse profiles were added in blocks lasting 10 minutes and for sub-bands of 128 MHz for NRT NUPPI, 150/125 MHz for the Effelsberg PSRIX data and 80 MHz

for the Lovell ROACH data (see Table 1). They were then cross-correlated with a low-noise template using the Fourier routine described in [Taylor \(1992\)](#) and implemented in the “PAT” routine of `PSRCHIVE` to derive the topocentric pulse times of arrival (TOAs). We then used `tempo`³ to correct the TOAs using the telescopes’ clock corrections and to convert them to the Solar System barycenter. This program reports all time-like units in Dynamical Barycentric time. To do this, the motion of the radio telescopes relative to the Earth was calculated using the data from the International Earth Rotation Service, and to the barycenter using the DE430 solar system ephemeris ([Folkner et al. 2014](#)). Finally, the differences between the measured TOAs and the predictions of our timing model (the *residuals*) were minimized using `tempo` by varying the parameters in the model, with and without a position fit. The parameters that best fit the data are presented in Table 2. To model the binary orbit, we used the DD model described by [Damour & Deruelle \(1985, 1986\)](#). These use the “range” (r) and “shape” (s) parameters to quantify the Shapiro delay; for high inclinations their correlation as small as those of the orthometric amplitude h_3 and ratio ς in the orthometric parameterization of the Shapiro delay ([Freire & Wex 2010](#)).

The residuals associated with the best-fit model are displayed in Figure 2. This timing model fits for right ascension (α) and declination (δ), with no trends detectable in the residuals. The residual root mean square (rms) for the overall solution is 3.48μ s, this represents a fraction of $\sim 10^{-4}$ of the spin period. For the individual observing systems the residual rms are presented in Table 1, where we also listed the times added in quadrature (EQUAD) to each data set in order

³ <http://tempo.sourceforge.net/>

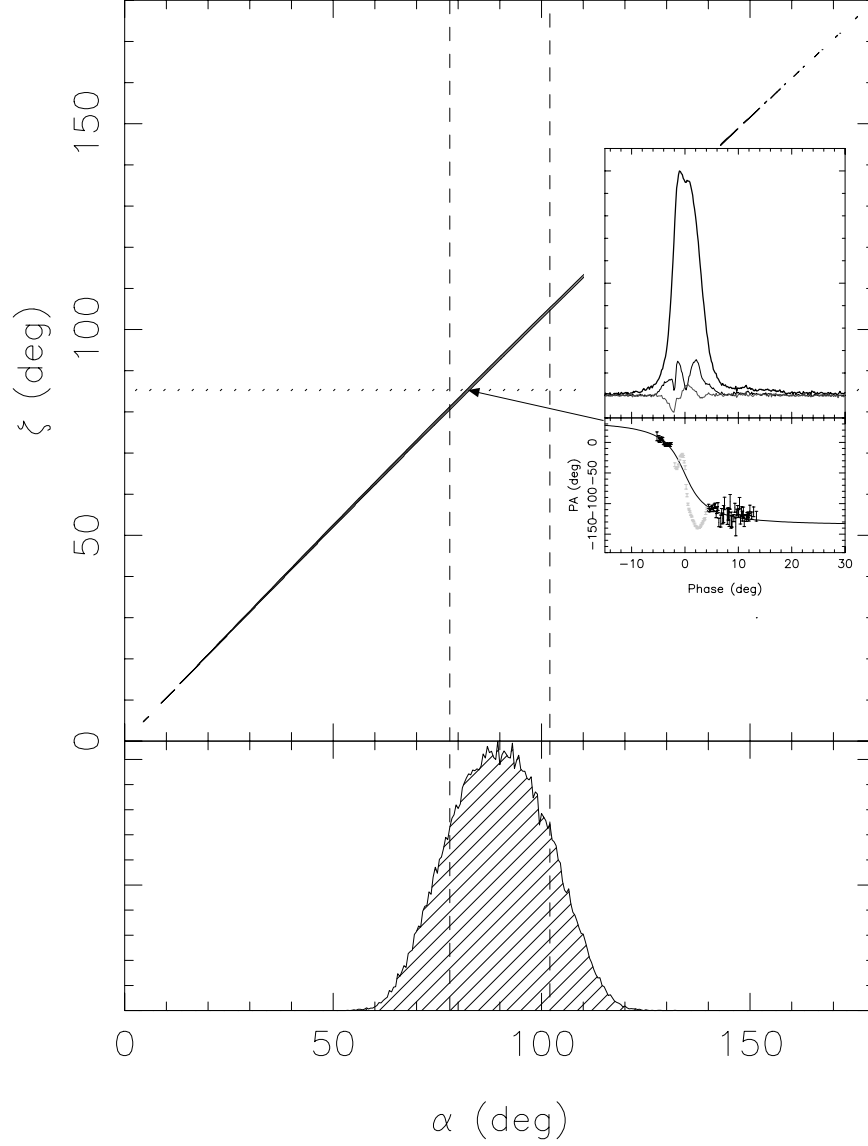


Figure 1. System geometry for PSR J2222–0137 as derived from a least-squares-fit of the Rotating Vector Model (RVM) to the PA of the linearly polarized emission. The top panel shows the regions of the magnetic inclination angle (α) and viewing angle (ζ) plane with the best RVM fits (see inset and text for details). We also mark the constraint on the orbital inclination angle as an horizontal strip. Also, assuming a filled emission beam, we derive a distribution of inclination angles (lower panel) that is consistent with the observed pulse width (see text for details). The vertical dashed lines indicate a $\pm 12^\circ$ band around 90° . For the point that satisfies the polarimetric and orbital inclinations constraints ($\alpha = 83^\circ$ and $\zeta = 85.27^\circ$) we calculate the RVM PA versus phase curve and superpose it on the measurements (see bottom plot of inset).

to achieve a reduced χ^2 of 1. This procedure results in more conservative uncertainty estimates for all timing parameters.

3. ASTROMETRY

We now discuss the astrometric parameters derived from timing. First, we fitted for parallax, proper motion and position simultaneously. In this way, we were able to make an independent measurement of these parameters using only our data set, i.e., not taking into account the early VLBI position (since there might be systematic offsets between the positions at the reference epoch). For the parallax we obtained a value of 3.88 ± 0.31 milliarcseconds (mas), which is consistent with VLBI parallax ($3.742^{+0.013}_{-0.016}$ mas). Since the latter is ~ 20 times more precise, we kept it fixed in all subsequent work.

We then fitted for proper motion, still fitting for position at the same time. Doing this, we obtained $\mu_\alpha = 45.00 \pm 0.21 \text{ mas yr}^{-1}$ and $\mu_\delta = -6.35 \pm 0.47 \text{ mas yr}^{-1}$. Both values are $\sim 1\text{-}\sigma$ consistent with the proper motions from Paper II, however the latter are still more precise by an order of magnitude; for this reason we used the VLBI proper motions in all subsequent fits.

Finally, we kept the parallax and proper motion fixed at the VLBI values and fitted for right ascension (α) and declination (δ), we obtained $\alpha = 22^{\text{h}} 22^{\text{m}} 05^{\text{s}} 969080(13)$ and $\delta = -01^\circ 37' 15'' 7262(5)$ for MJD = 55743; these represent offsets of $d\alpha = 0.000021(13)$ seconds and $d\delta = -1.8 \pm 0.5$ mas relative the VLBI position. This means the timing position in α is $2\text{-}\sigma$ consistent with the α from VLBI, but in δ the offset is nearly $4\text{-}\sigma$ significant: fitting for the position produces a large reduction in the χ^2 of the fit (from 3076.9 to 2874.0). This reduction is too large to ignore, so we investigated the reasons for this.

1. We use the same epoch for the position as the epoch quoted in Paper II, thus verifying that the proper motion is not the cause of the positional offset.
2. This offset is not due to any misalignment of the reference frames: According to Folkner et al. (2014), the DE430 reference frame is aligned to the International Celestial Reference frame to better than 0.2 mas (10 times smaller than the measured offset). Nor is it caused by shortcoming of tempo: A fit with tempo2 (Hobbs et al. 2006; Edwards et al. 2006) results in a very similar offset.
3. Since the pulsar is within 8 degrees of the Ecliptic, we have investigated whether the solar wind might have a significant effect on the timing. The position of the pulsar can change significantly with the assumed solar wind density parameter, but in no case does it match the VLBI position. Furthermore, density parameters

for the solar wind higher than 10 cm^{-3} cause a significant degradation in the timing model.

4. Nevertheless, it is known that the solar wind density changes with time, implying that, to time a pulsar near the ecliptic properly, one would in principle need to know how the solar wind density changes with time. This information is not readily available. To avoid this problem, we adopted the common practice in pulsar timing arrays (PTAs) and excluded all TOAs where the Sun is within 15° of the pulsar, i.e., where the Ecliptic longitude of the Sun λ_\odot is within 12.7444° of the longitude of the pulsar, $\lambda_{\text{PSR}} = 336.7319^\circ$. This corresponds to any days from Feb. 13 to March 11. Doing this does not change the positional offset.
5. Independently of this, many pulsars show variations in their DMs caused by their motions relative to the Earth. The line of sight to the pulsar goes through varying electron column densities, causing an irregular (and unpredictable) change in their DMs. These changes affect especially timing parameters with a long signature, like the astrometric parameters. If we model DM variations using a piecewise-constant function (the so-called “DMX” model, Demorest et al. 2013) and keep the VLBI positions, we can see an apparently yearly change in the DM. However, if we used the DMX model *and* fit for position, then we see that the best fit is where the position changes and the DMs change approximately linearly with time, with no sign of a yearly modulation. This means that when we used the DMX model and kept the VLBI position, the DM coefficients were in effect absorbing the yearly residuals.

Given this situation, we conclude that a) we get a perfect agreement with the parallax, and a reasonable agreement with the proper motion in Paper II, b) the positional offset we found is qualitatively and quantitatively robust, and that c) it is not an effect of DM variations, caused by the Sun or otherwise. The latter point is corroborated by the fact that our measurement of parallax coincides with the parallax measurement in Paper II; the parallax is the parameter that suffers most from timing systematics with a yearly signature.

Could some systematic effects have affected the VLBI parallax? According to A. Deller (2017, private communication), there are two potential sources of error that were neglected in Paper II by the assumption that the out-of-beam calibrator position uncertainty dominates the target absolute position uncertainty:

1. Core-shift in the out-of-beam calibrator J2218–0335 (since its position is defined at 2.3/8.4 GHz, and the PSR J2222–0137 measurements were done at 1.6

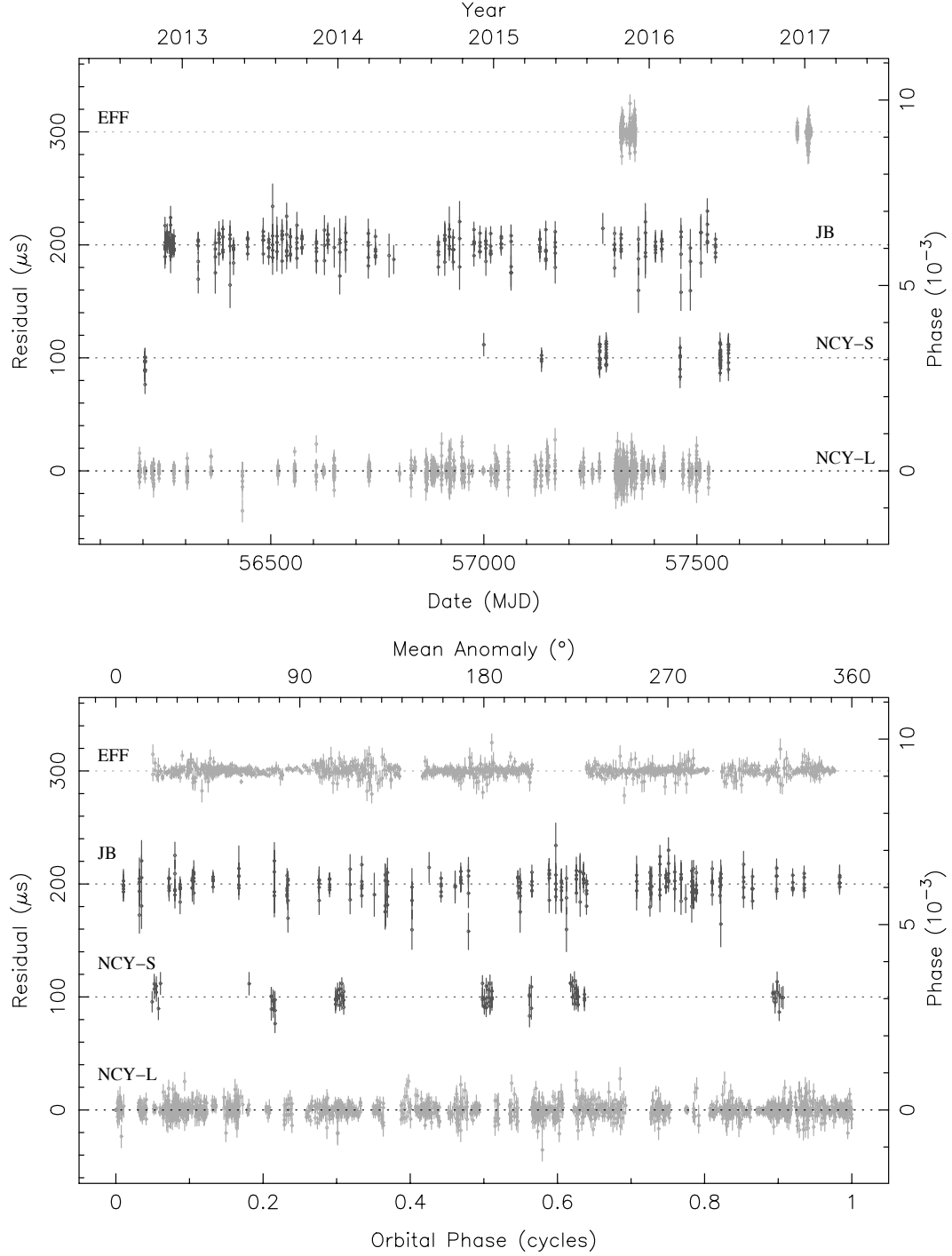


Figure 2. Timing residuals (measured pulse arrival times – model pulse arrival times) as a function of MJD (top) and mean anomaly (bottom) for the timing solution of PSR J2222–0137 where we fit for position. The residuals are displayed with different offsets for each instrument. No trends are noticeable in the residuals, indicating that the model describes the topocentric pulse times of arrival (TOAs) well. EFF - Effelsberg TOAs, JB - Lovell telescope (Jodrell Bank), NCY-S - Nançay at S-band and NCY-L - Nançay at L-band.

GHz). This error cannot be evaluated precisely - that would require a careful, multi-frequency/multi-calibrator campaign - but potentially it could provide a shift of the order of 1 mas (Sokolovsky et al. 2011).

2. Errors in the residual phase-referencing errors from the out-of-beam calibrator to the in-beam calibrator. The angular separation here is $\sim 2^\circ$, which could originate an error of ~ 1 -2 mas in a typical observation, but could be even more if ionospheric conditions are unfavorable. This effect should average out, but a fraction of a mas is to be expected for the final position. Again, verifying this would require a careful, multi-frequency/multi-calibrator campaign.

These contributions are systematically taken into account in recent publications. As an example, Deller et al. (2016) estimated an absolute uncertainty of the in-beam calibrator for PSR J2145–0759 of about 2.5 mas. This should be smaller for PSR J2222–0137 because the distance between pulsar and calibrator is 30% smaller and the latter pulsar is not so far South, but nevertheless it is conceivable that these effects could produce an offset similar to what we observe (~ 2 mas), although without a dedicated multi-frequency/multi-calibrator campaign it will not be possible to quantify this more precisely. Nevertheless, these recent uncertainty estimates show that the 0.1 mas precision for the absolute position claimed in Paper II is too optimistic.

In any case, the two timing solutions presented in Table 2 – one using the VLBI position and the other using our best fit position – show that the Shapiro delay parameters and the orbital variability parameters change by 1σ or less with these different positions, i.e., the masses derived in this paper are consistent for these two positions.

4. TIMING RESULTS

In Table 2, we present our main results, the timing parameters for PSR J2222–0137. As mentioned in Section 3, we have discarded all TOAs taken when the Sun is at an angular distance from the pulsar smaller than 15 degrees. Furthermore, as mentioned in the previous section, when we fit for position and use the DMX model, we see a steady secular increase in the DM, for this reason we decided to model the DM evolution with a DM and DM derivative only. In a later stage we turn off the fit for both DM and its derivative since we also fit for the FD parameters (Arzoumanian et al. 2015) - If all of these parameters are fit together, the DM can easily change to unrealistically large or small (sometimes negative) values. The uncertainties presented are 68% (1σ equivalent) confidence limits derived by `tempo`. We now discuss the significance of some of these parameters.

4.1. Spin parameters

The spin properties for this pulsar were discussed in Paper I. Most of the observed spin period derivative, ($\dot{P} = 5.80 \times 10^{-20}$) results from kinematic contributions. Once those are subtracted, the resulting intrinsic spin-down is $\dot{P}_{\text{int}} = 1.75 \times 10^{-20} \text{ s s}^{-1}$. This is slightly larger than the value presented in Paper I because, apart from correcting for the Shklovskii effect (Shklovskii 1970), we also correct for the difference in Galactic accelerations of PSR J2222–0137 and the Solar System (Damour & Taylor 1991) using the latest model for the rotation of the Galaxy (Reid et al. 2014). However, the latter is a small term that does not change any of the basic conclusions: a characteristic age $\tau_c = P/(2\dot{P}_{\text{int}}) \sim 30$ Gyr and a relatively small B-field ($B_0 = 3.19 \times 10^{19} \text{ G} \sqrt{P\dot{P}_{\text{int}}} = 7.6 \times 10^8 \text{ G}$; see e.g., Lorimer & Kramer 2004).

4.2. Shapiro delay

The masses of the components of the binary can be determined reasonably well using the Shapiro delay alone: we obtain $m_p = 1.76(6)M_\odot$, $m_c = 1.293(25)M_\odot$ and $i = 85.27(22)^\circ$ or $i' = 94.73(22)^\circ$. If we don't fit for the position, the masses are 1σ larger (see Table 2).

In order to verify these values and their uncertainties we have made a χ^2 map of the $\cos i - m_c$ space. At each point, we fix the Shapiro delay values and fit for all other parameters, recording the χ^2 for each fit. From this χ^2 map we derive a 2-D probability density map (see Fig. 3) according to the Bayesian procedure described in Splaver et al. (2002), see e.g., Barr et al. (2017) for details. From this, we obtain $m_p = 1.760^{+0.063}_{-0.061} M_\odot$, $m_c = 1.293^{+0.025}_{-0.024} M_\odot$ and $i = 85.27(21)^\circ$ (or $i' = 94.73(21)^\circ$). A bootstrap Monte-Carlo estimate yields smaller uncertainties, e.g., $m_c = 1.293(17)M_\odot$, for this reason we keep the `tempo` estimate since it is more conservative. These values are not consistent with the masses published in Paper I, in terms of the latter's estimated values and 1σ uncertainties, they are both 4σ too large. It is important to understand the reason for this difference.

We begin by pointing out that we have made a substantially larger number of measurements with much better orbital coverage over a more extended period of time, all of which are important not only for improving the precision of the Shapiro delay, but also for reducing the correlations between different parameters. One of these correlations is especially important, and had already been explicitly mentioned in Paper I: it is the correlation between the Shapiro delay parameters and the rate of advance of periastron, $\dot{\omega}$. Indeed, in Paper I, when the authors fit for $\dot{\omega}$, they obtain a significant improvement in the quality of their fit (an early indication that the effect is measurable) and an increase in the masses derived from the Shapiro delay by about 1σ compared to their tabulated value (where this effect was not taken into account). This leads us to conclude that our measurement of $\dot{\omega}$ is one of the main

Table 2. Parameters for the PSR J2222–0137 binary pulsar

General timing parameters		
Right Ascension, α (J2000)	22:22:05.969101 (a)	22:22:05.969080(13)
Declination, δ (J2000)	−01:37:15.72441 (a)	−01:37:15.7262(5)
Proper motion in α , μ_α (mas yr ^{−1})	44.73 (a)	44.73 (a)
Proper motion in δ , μ_δ (mas yr ^{−1})	−5.68 (a)	−5.68 (a)
Parallax, π_x (mas)	3.742 (a)	3.742 (a)
Spin frequency, ν (Hz)	30.47121380904560(27)	30.47121380904550(29)
Spin frequency derivative, $\dot{\nu}$ (10 ^{−18} Hz s ^{−1})	−5.38780(28)	−5.38746(34)
Dispersion Measure, DM (pc cm ^{−3})	3.277	3.277
DM derivative, DM1 (pc cm ^{−3} yr ^{−1})	0.00082	0.00082
FD1	−0.00135(14)	−0.00131(13)
FD2	0.0048(4)	0.0046(4)
FD3	−0.0069(6)	−0.0068(6)
FD4	0.00331(28)	0.00323(26)
Rotation Measure, RM (rad m ^{−2})	2.6(1) (b)	2.6(1) (b)
Weighted residual rms (μ s)	3.481	3.365
χ^2	3076.9	2874.0
Reduced χ^2	1.076	1.006
Binary Parameters		
Orbital Period, P_b (days)	2.44576456(13)	2.44576469(13)
Projected Semi-major Axis of the pulsar orbit, x (lt-s)	10.8480229(6)	10.8480239(6)
Epoch of Periastron, T_0 (MJD)	56001.38392(7)	56001.38381(8)
Orbital Eccentricity, e	0.000380940(3)	0.000380967(30)
Longitude of Periastron, ω (°)	119.916(11)	119.900(11)
Rate of advance of Periastron, $\dot{\omega}$	0.1004(28)	0.1033(29)
Shapiro delay "shape" s	0.99669(29)	0.99659(30)
Shapiro delay "range" r (M_\odot)	1.323(25)	1.293(25)
Variation of P_b , $\dot{P}_{b,obs}$ (10 ^{−12} s s ^{−1})	0.27(9)	0.20(9)
Variation of x , \dot{x} (10 ^{−15} lt-s s ^{−1})	7.8(30)	3.5(30)
Position angle (PA) of line of nodes, Ω (°, J2000) ...		5 ⁺¹⁵ _{−20} (a)
Derived Parameters		
Galactic Longitude, l (°)		62.0184
Galactic Latitude, b (°)		−46.0753
Ecliptic Longitude, λ (°)		336.7319
Ecliptic Latitude, β (°)		7.9771
Distance, d (pc)		267.3 (a)
Total proper motion, μ_T (mas yr ^{−1})		45.09(2) (a)
PA of proper motion, Θ_μ (°, J2000)		97.23 (a)
Transverse velocity, v_T (km s ^{−1})		57.1 ^{+0.3} _{−0.2} (a)
Pulsar Spin Period, P (s)	0.03281785905434272(30)	0.03281785905434283(31)
Spin Period Derivative, \dot{P} (10 ^{−21} s s ^{−1})	58.0272(30)	58.0236(36)
Intrinsic Period Derivative, \dot{P}_{int} (10 ^{−21} s s ^{−1})		17.50
Surface Magnetic Field Strength, B_0 (10 ⁹ G)		0.76
Characteristic Age, τ_c (Gyr)		29.7
Spin-down energy, \dot{E} (10 ³⁰ erg s ^{−1})		19.5
Mass function, f (M_\odot)	0.22914228(4)	0.22914232(4)
Pulsar mass, m_p (M_\odot)	1.84(6)	1.76(6)
Total binary mass, M (M_\odot)	3.16(8)	3.05(9)
Orbital inclination, i (°)	85.34(21)	85.27(22)
Intrinsic \dot{P}_b , $\dot{P}_{b,int}$ (10 ^{−12} s s ^{−1})	+0.01(9)	−0.06(9)

NOTE—Timing parameters derived using tempo. The left column is the timing solution derived using the position from Paper II. The right column is the timing solution where we fit for position (α and δ). The reference epoch is MJD = 56000, the position epoch is for MJD = 55743, as in Paper II. We use the DE 430 Solar System ephemeris, time units are in barycentric dynamic time (TDB). The FDN parameters model non-dispersive changes in the average residual with frequency (Arzoumanian et al. 2015). The binary parameters derived from the timing (all but Ω) are relative to the DD orbital model. Numbers in parentheses represent 1- σ uncertainties in the last digits as determined by the timing programs, scaled such that the reduced $\chi^2 = 1$. (a) Value determined from VLBI measurements. (b) Value from Paper I.

reasons for the large difference in the Shapiro delay measurements.

4.3. Advance of periastron

In this timing campaign, we have measured $\dot{\omega}$ with high (35σ) significance: $\dot{\omega}_{\text{obs}} = 0.1033(29)^\circ\text{yr}^{-1}$. Given the optical non-detection of the companion to PSR J2222–0137, it is clear that it must be a highly compact object. Like the pulsar, it will behave essentially like a point mass. This means that “classical” rotational or tidal contributions to the observed $\dot{\omega}$ should be absent. Therefore, $\dot{\omega}_{\text{obs}}$ should be dominated by the relativistic contribution, with an insignificant contribution from kinematic effects (section 4.4).

For all known systems where the masses can be determined independently, general relativity (GR) provides an accurate prediction of this quantity; to leading post-Newtonian order it depends only on the Keplerian parameters and the total mass of the system M , in solar masses (Robertson 1938; Taylor & Weisberg 1982):

$$\dot{\omega}_{\text{GR}} = 3 \frac{(MT_\odot)^{2/3}}{1-e^2} \left(\frac{P_b}{2\pi} \right)^{-5/3}, \quad (1)$$

where $T_\odot \equiv (\mathcal{GM})_\odot^N c^{-3} = 4.9254909476412675(\dots)\mu\text{s}$ is the nominal solar mass parameter⁴ in time units, c is the speed of light. Using the M presented in Paper I, we should expect $\dot{\omega}_{\text{GR},1} = 0.077^\circ\text{yr}^{-1}$; for the M presented in this paper ($3.05(9)M_\odot$) we should expect $\dot{\omega}_{\text{GR},2} = 0.0943^\circ\text{yr}^{-1}$. The observed value is about 3σ above $\dot{\omega}_{\text{GR},2}$, while it is 9σ above $\dot{\omega}_{\text{GR},1}$. This is an independent indication that the larger masses derived in this paper are closer to the real value, however the agreement with $\dot{\omega}_{\text{GR},2}$ is not very good either. We should keep in mind that for low-eccentricity orbits this quantity is easily affected by systematic effects. As an example of this, if we use the DMX model and fit for position then we obtain $\dot{\omega}_{\text{obs}} = 0.1006(35)^\circ\text{yr}^{-1}$, if we don’t fit for position then $\dot{\omega}_{\text{obs}} = 0.1001(35)^\circ\text{yr}^{-1}$, these values are 1σ smaller; they are only 1.7σ above $\dot{\omega}_{\text{GR},2}$. As a comparison, the Shapiro delay masses vary by only $\pm 0.1\sigma$ respectively.

We can in principle combine $\dot{\omega}_{\text{obs}}$ with the Shapiro delay to obtain self-consistent GR mass measurements, using the DDGR model (Damour & Deruelle 1986). However, because we believe that the $\dot{\omega}_{\text{obs}}$ is currently contaminated by systematic effects, we don’t regard the result of such a fit as being reliable.

⁴ Although neither G nor the mass of the Sun (M_\odot) are known to better than 4 decimal places, their product is known to more than nine decimal places. Recently, the IAU 2015 Resolution B3 has defined the *nominal solar mass parameter*, denoted by $(\mathcal{GM})_\odot^N$, to be exactly $1.3271244 \times 10^{20} \text{ m}^3 \text{ s}^{-2}$. Thus the value for T_\odot as defined above is also exact, it is no longer tied to the actual (time-varying) mass of the Sun, but instead to the SI units of time and length.

However, this situation will change. As we extend our timing baseline T the uncertainty of $\dot{\omega}_{\text{obs}}$ will decrease at a rate given by $T^{-3/2}$; we also expect that the relative contribution from systematic effects will decrease. This means that a self-consistent combination of $\dot{\omega}_{\text{obs}}$ with the Shapiro delay will provide much more precise masses in the future, as for PSRs J1903+0327, J1807–2500B, J0453+1559 and J1946+3417 (Freire et al. 2011; Lynch et al. 2012; Martinez et al. 2015; Barr et al. 2017).

4.4. Kinematic effects

Given the well-known values for distance and proper motion, we can estimate the kinematic contributions to the observed variations of P_b (Shklovskii 1970; Damour & Taylor 1991), x and ω (Arzoumanian et al. 1996; Kopeikin 1996).

4.4.1. Variation of the orbital period

For \dot{P}_b , we expect a kinematic contribution of $\dot{P}_{b,k} = 0.2648(17) \times 10^{-12} \text{ s s}^{-1}$, which is due to the Shklovskii effect ($\dot{P}_{b,\text{Shk}} = 0.2790(11) \times 10^{-12} \text{ s s}^{-1}$ - the uncertainty here is dominated by the uncertainty in the distance to the system) and the Galactic acceleration ($\dot{P}_{b,\text{Gal}} = -0.0142(13) \times 10^{-12} \text{ s s}^{-1}$, where we assumed a 10% uncertainty in the vertical acceleration of the system). The GR prediction for the orbital decay caused by the emission of gravitational waves, $\dot{P}_{b,\text{GR}} = -0.0077(4) \times 10^{-12} \text{ s s}^{-1}$, is 34 times smaller than the kinematic contribution. The total predicted \dot{P}_b is then $\dot{P}_{b,p} = 0.2571(17) \times 10^{-12} \text{ s s}^{-1}$.

From our data we get $\dot{P}_{b,\text{obs}} = (0.20 \pm 0.09) \times 10^{-12} \text{ s s}^{-1}$, which is consistent with $\dot{P}_{b,p}$. Subtracting the expected kinematic contribution, we obtain the intrinsic component of the orbital variation, $\dot{P}_{b,\text{int}} = -0.063 \pm 0.085 \times 10^{-12} \text{ s s}^{-1}$. This is consistent, but not yet precise enough for a detection of the quadrupolar GW emission predicted by GR.

Subtracting the expected GR contribution, we obtain an excess of $\dot{P}_{b,\text{xs}} = -0.055 \pm 0.085 \times 10^{-12} \text{ s s}^{-1}$, which represents the upper limit for dipolar GW emission. As discussed in section 5, this is already small enough to introduce interesting constraints on the emission of dipolar gravitational waves from this system. Furthermore, these limits will improve fast since the uncertainty of \dot{P}_b decreases with $T^{-5/2}$.

4.4.2. Secular variation of the projected semi-major axis of the pulsar’s orbit

The expected kinematic effect on the projected semi-major axis of the pulsar’s orbit (x) is given by (Kopeikin 1996):

$$\frac{\dot{x}}{x} = \mu_T \cot i \sin(\Theta_\mu - \Omega), \quad (2)$$

where Θ_μ is the PA of the proper motion (97.23°) and Ω is the PA of the line of nodes; for these angles we use the “ob-

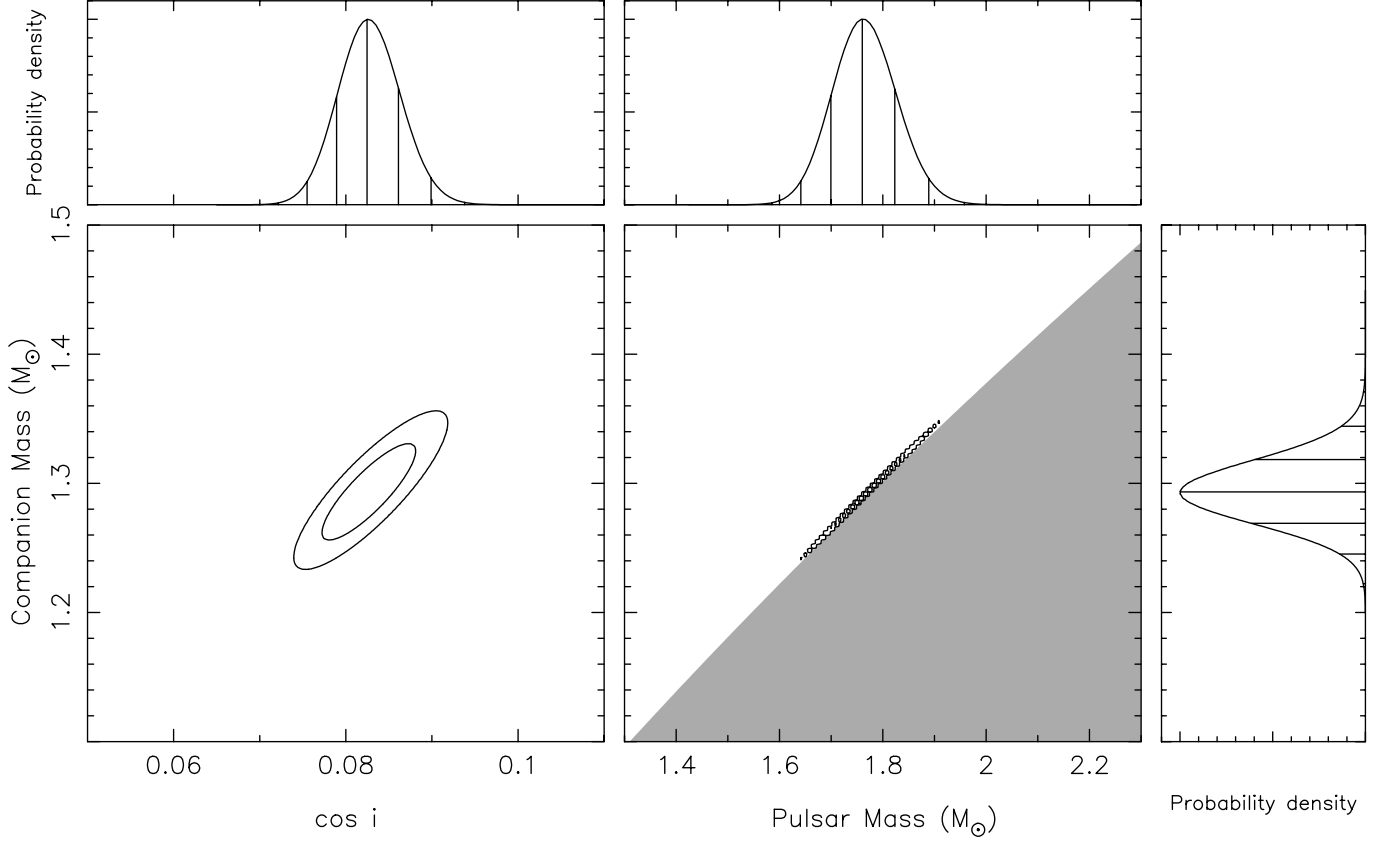


Figure 3. Current constraints from timing of PSR J2222–0137. The black, solid contour lines include 68.3 and 95.4% of the 2-D probability distribution function derived from our χ^2 maps (see text). *Left:* m_c - $\cos i$ plane. *Right:* m_c - m_p plane. The gray region is excluded by the mathematical constraint $\sin i \leq 1$. Top and side panels: 1-D probability distribution functions for $\cos i$, m_p and m_c , with median, 1, 2 and 3 σ equivalent percentiles indicated as vertical lines. The upper mass limit for a rigidly rotating WD is $1.48 M_\odot$.

server’s convention” mentioned in Section 2.1⁵. Despite the relatively large μ_T , the expected \dot{x} is relatively small mostly because i is close to 90° ; this implies that $\cot i$ term is also small. Nevertheless, our measurement of \dot{x} is already precise enough to start introducing some constraints. As mentioned in Section 1, Ω was measured in Paper II and is 5^{+15}_{-20} , this means that we should expect $\dot{x}_p = \pm 6.06 \times 10^{-15}$ lt-s s^{-1} , depending on whether $i = 85.27(22)^\circ$ or $i' = 94.73(22)^\circ$ respectively. The observed value, $\dot{x}_{\text{obs}} = +(3.5 \pm 3.0) \times 10^{-15}$ lt-s s^{-1} , is 1- σ consistent with the \dot{x}_p for i and 3.2 σ larger

than the \dot{x}_p for i' . From this we conclude that i is the more likely the orbital inclination.

The uncertainty in \dot{x}_{obs} decreases with $T^{-3/2}$; this implies that soon it will provide a choice of the orbital inclination with much higher confidence.

4.4.3. Annual orbital parallax

Apart from the secular variation of \dot{x} there is another kinematic effect on x , the annual orbital parallax. This is a yearly modulation of x caused by the the changing viewing angle of the pulsar’s orbit due to the Earth’s orbital motion (Kopeikin 1996).

The DDK orbital model in `tempo` can fit for this and other annual effects, like the orbital parallax, but it automatically takes \dot{x} into account. It is therefore not easy to separate the constraints introduced by the annual orbital parallax from the

⁵ In Freire et al. (2011), eq. 2 has a minus sign, which corresponds to a convention where PAs are measured from North through East and a binary system with an orbital inclination of 0° has its angular momentum pointing away from us. Such a convention is left handed, the convention used here is right handed.

constraints introduced by \dot{x} . Nevertheless, a fit for Ω using the DDK model yields $\Omega = (320 \pm 104)^\circ$. While consistent with the measurement of Ω in Paper II, this is not very restrictive, i.e., we see no sign of a constraint on Ω introduced by the annual orbital parallax beyond the constraints already introduced by the measurement of \dot{x} .

This is not surprising: this is a very small effect that has only been detected for pulsars with extremely high timing precision like PSRs J0437–4715, J1713+0747 and J1909–3744 (Reardon et al. 2016; Fonseca et al. 2016; Desvignes et al. 2016). However, given its combination of small distance and relatively large orbital size, PSR J2222–0137 is a candidate for the detection of this effect, particularly if it can be observed with more sensitive telescopes. Since Arecibo is not an option (the pulsar is just below that telescope’s Southern limit) this will only be possible with FAST (Smits et al. 2009) or the SKA (Shao et al. 2015).

Since the DDK model introduces new orbital effects, it is important to verify whether they have an impact on other orbital parameters. The answer is no: the Shapiro delay masses obtained with this model are 0.15σ smaller and the $\dot{\omega}_{\text{obs}}$ is 0.2σ smaller compared to the values from the DD model, whether we assume the VLBI Ω or not. The astrometry is unchanged. As the timing precision improves, it will be essential to do this correction, and for that the VLBI measurements are very important.

4.4.4. Contribution to the observed periastron advance

Since the observed $\dot{\omega}$ appears to be slightly larger than the GR expectation, it is important to know whether there are extra contributions to this effect that have not been taken into account.

Given the large proper motion of the system, there will be a kinematic contribution to $\dot{\omega}$ caused by the changing viewing geometry, this is given by:

$$\dot{\omega}_K = \frac{\mu_T}{\sin i} \cos(\Theta_\mu - \Omega), \quad (3)$$

where all quantities are as in the equation above. Thus $\dot{\omega}_K = -0.5_{-4.3}^{+3.3} \times 10^{-6} \text{ yr}^{-1}$. Even if we had no constraints whatsoever on Ω , we would still have $|\dot{\omega}_K| \leq 1.25 \times 10^{-5} \text{ yr}^{-1}$. This is more than two orders of magnitude smaller than the measurement uncertainty of $\dot{\omega}_{\text{obs}}$, $2.9 \times 10^{-3} \text{ yr}^{-1}$. We thus conclude that this is not the reason for the larger than expected value of $\dot{\omega}$.

5. PSR J2222–0137 AS A GRAVITATIONAL WAVE LABORATORY

The large difference in compactness between a NS and a WD makes pulsar-WD binaries ideal laboratories for gravity theories that violate the strong equivalence principle (Shao &

Wex 2016). In such alternatives to GR, the leading contribution in the loss of orbital energy by gravitational waves, generally, comes from dipolar radiation. The radiation reaction of dipolar waves enters the equations of motion of a binary system already at the 1.5 post-Newtonian level (i.e. order v^3/c^3), and is therefore expected to dominate the damping of the orbit in systems like PSR J2222–0137. For the scalar-tensor theories, like the ones studied in Damour & Esposito-Farèse (1992, 1993), one finds for the change in the orbital period by dipolar radiation damping

$$\dot{P}_b^D = -2\pi \frac{G_*}{c^3} \frac{m_p m_c}{m_p + m_c} \left(\frac{P_b}{2\pi} \right)^{-1} \frac{1 + e^2/2}{(1 - e^2)^{5/2}} (\alpha_p - \alpha_c)^2, \quad (4)$$

where G_* denotes the bare gravitational constant, and α_p and α_c are the effective scalar couplings of pulsar and companion respectively. In the discussion here, for simplicity, we will mostly refer to the mono-scalar-tensor theory investigated in detail in Damour & Esposito-Farèse (1993, 1996). Nevertheless, the (generic) limits we present below apply to a wider class of scalar-tensor theories, and to some extent to a large range of gravity theories with dipolar radiation. The quantities α_p and α_c in equation (4) have a (non-linear) dependence on the bodies’ gravitational binding energy. For the weakly self-gravitating WD companion the effective scalar coupling can be approximated by the linear matter-scalar coupling constant, i.e. $\alpha_c \approx \alpha_0$. In the meantime, a Solar System experiment (Bertotti et al. 2003) constrains $|\alpha_0| \lesssim 0.003$ (Will 2014). The pulsar’s effective scalar coupling α_p , on the other hand, may be of order one, even for a vanishing α_0 (Damour & Esposito-Farèse 1993). Given the uncertainties in the masses of PSR J2222–0137, we can safely approximate G_* by Newton’s gravitational constant $G \equiv G_*(1 + \alpha_0^2)$, and use T_\odot instead of $G_* M_\odot / c^3$ in equation (4). Inserting the numbers from Table 2 into equation (4) gives

$$\dot{P}_b^D = -(697 \pm 19) \times 10^{-12} (\alpha_p - \alpha_0)^2. \quad (5)$$

In case of a strongly scalarized PSR J2222–0137 ($\alpha_p \sim 1$) equation (5) gives an orbital decay that is in conflict with the derived intrinsic change of the orbital period ($\dot{P}_{b,\text{int}}$ in table 2) by about four orders of magnitude. In turn, this implies a tight upper limit on the scalar charge of PSR J2222–0137. A detailed analysis, which properly accounts for all the uncertainties and correlations through Monte Carlo simulations, gives the following (generic) limit

$$|\alpha_p| < 0.02 \quad (95\% \text{ C.L.}). \quad (6)$$

Since the masses for the PSR J2222–0137 are derived from the Shapiro delay, caused by the (weakly self-gravitating) WD companion, one also has to account for a modification of the gravitational constant in the mass function (see equation 5.8 in Damour & Esposito-Farèse 1996). However, this

strong-field modification is sub-leading in our test, since in the PSR J2222–0137 system the effective gravitational constant is given by $G_*(1 + \alpha_p \alpha_0)$, and $|\alpha_0| \ll 1$.

The limit from equation (6) is an order of magnitude weaker than the limit derived for PSR J1738+0333 ($1.46 M_\odot$) in Freire et al. (2012) and still a factor of four weaker than the limit derived by Antoniadis et al. (2013) for PSR J0348+0432 ($2.0 M_\odot$). However as first pointed out by Shibata et al. (2014), depending on the EoS, a $\sim 1.8 M_\odot$ could still be strongly scalarized, in spite of the tight limits at 1.46 and $2.0 M_\odot$. Because of this, the limit given above has its own importance. In fact, in a recent analysis, Shao et al. (2017) have used a set of pulsars with different masses, in order to place the best constraints on such strong field scalarization, for a wide range of EoS. Such constraints, as discussed by these authors, are of great importance for LIGO, Virgo and future gravitational wave observatories. The limit of PSR J2222–0137 makes, because of the pulsar’s mass, an important contribution to the constraints of Shao et al. (2017).

The precision of this test will improve greatly in the future: First, because m_p and m_c will be much better known; this is important for the interpretation of the experiment, in particular for a precise calculation of the expected \dot{P}_b from dipolar GWs⁶: For some equations of state (and some scalar-tensor theories of gravity), the dipolar term varies extremely rapidly with m_p , so its precise measurement is very important. Second, because, as mentioned above, the uncertainty of \dot{P}_b ($\delta\dot{P}_b$), decreases with $T^{-5/2}$, so a factor of ~ 10 improvement (i.e., $\delta\dot{P}_{b,\text{obs}} = 0.008 \times 10^{-12} \text{ s s}^{-1}$) will be achieved when our timing baseline is 10 years long (i.e., within 6 years from now). A factor of 50 improvement over the current limit ($\delta\dot{P}_{b,\text{obs}} = 0.0016 \times 10^{-12} \text{ s s}^{-1}$) would require a total timing baseline of 19 years, i.e., it will be achieved in about 15 years. This can be significantly reduced if a much more sensitive radio telescope is used to time the pulsar, like the SKA (Shao et al. 2015). At that time the precision on $\dot{P}_{b,\text{obs}}$ will be similar to the current uncertainty from kinematic contributions (see Subsection 4.4.1) and we will have a limit on α_p for this pulsar similar to that derived for PSR J1738+0333. However, the better models of the Galactic potential that will result from the GAIA mission and the much improved distance measurements that will be made possible with the SKA should allow a significant improvement in the estimate of the kinematic terms, which will translate directly into an improvement of the precision of this experiment.

6. MODELLING THE FORMATION OF PSR J2222–0137

⁶ The uncertainty on \dot{P}_b from the quadrupolar GR contribution $\dot{P}_{b,\text{GR}}$ is already so small that we can ignore it; improvements in the mass measurements will further reduce the uncertainty of this quantity in the future.

Despite the relatively massive compact objects in this binary, the formation of PSR J2222–0137 is expected to resemble the standard scenario for forming binaries with recycled pulsars and massive WDs (e.g. Tauris et al. 2012). The zero-age main sequence (ZAMS) progenitor system of PSR J2222–0137 may have contained two ZAMS stars with a primary mass of $20 - 25 M_\odot$ and a secondary mass of $6 - 8 M_\odot$ (see discussion below). Assuming this binary formed a common envelope (CE, Ivanova et al. 2013) once the primary star became a giant star and initiated mass transfer, the secondary star was unable to accrete much material and its mass may have remained roughly constant until the supernova (SN) explosion of the naked core of the primary star. After the formation of the NS, the system briefly becomes an intermediate-mass X-ray binary (IMXB) when its relatively massive companion star fills its Roche lobe and starts transferring mass to the NS (via Roche-lobe overflow, or RLO). As a consequence of the large mass-ratio ($q \simeq 3 - 4$) between the donor star and the accreting NS, the mass transfer becomes dynamically unstable and leads to the formation of a second CE in which the hydrogen-rich layer is removed from the companion star and a naked helium star is formed.

The further evolution of such NS-helium star binaries leads to a final phase of mass transfer (so-called Case BB RLO) once the helium star becomes a giant star, e.g. Habets (1986), Dewi et al. (2002), Ivanova et al. (2003), Tauris et al. (2012), Lazarus et al. (2014), and Tauris et al. (2015). Here we follow the method of detailed modelling outlined in Lazarus et al. (2014).

For the progenitor of the massive $1.293 \pm 0.025 M_\odot$ ONeMg WD we find that the mass of the helium star was $2.4 - 2.5 M_\odot$. The orbital period prior to Case BB RLO was about 1.2-1.3 days and the total duration of this mass-transfer phase was only ≤ 20000 yr. This rapid phase of recycling combined with the current spin period of 32 ms places some interesting constraints on the accretion efficiency of the NS. Before illuminating the accretion history, we first discuss the WD cooling age and the spin history of this pulsar.

6.1. Spin-down history of the pulsar and cooling age of the companion

Following Paper I, we use the WD cooling tracks of Bergeron et al. (2011) to estimate its age. The most massive WD listed in their tables⁷ has a mass of $1.30 M_\odot$, consistent with our estimate for the companion of PSR J2222–0137. This massive WD cools down to a surface temperature below 3000 K in 3.4 to 4.7 Gyr, depending on the hydrogen content in the outer layers. Given the non-detection of the companion of PSR J2222–0137, however, the end of the re-

⁷ <http://www.astro.umontreal.ca/~bergeron/CoolingModels/>

cycling phase could have occurred a longer time ago – in principle, between 3.4 and 13 Gyr. We note that the larger mass estimate of the WD implies that the system is not necessarily as old as implied in Paper I. For a $1.05 M_{\odot}$ CO WD (the WD mass estimate from Paper I), the cooling tracks of Bergeron et al. (2011) reach $T_{\text{eff}} = 3000 \text{ K}$ in 7.4 to 9.7 Gyr. Therefore, a $1.30 M_{\odot}$ ONeMg WD cools to this temperature 4–5 Gyr faster than a $1.05 M_{\odot}$ WD (which probably has a CO composition interior instead, although this difference in chemical composition should not affect the cooling timescale by much).

From the observed spin period (32.8 ms) and period derivative ($\dot{P}_{\text{int}} = 1.75 \times 10^{-20}$), we can probe the spin-down history of PSR J2222–0137 given the above cooling age constraint from the ONeMg WD (cf. Section 5.1.1 in Lazarus et al. 2014). Assuming a standard spin evolution with a braking index of $n = 3$, we find an initial P (after recycling) of 30 ms and 25 ms, for an age of 3.4 Gyr and 12.4 Gyr, respectively. The limited slow down of the spin period, even on a Hubble time, is caused by the relatively small B-field of this pulsar; it implies that after recycling the pulsar had a spin period similar to what it has today. This is useful when probing the accretion history of the system.

6.2. Accretion history and NS birth mass of PSR J2222–0137

If the accretion rate onto the NS is limited by the Eddington luminosity, the NS is only able to accrete $7\text{--}8 \times 10^{-4} M_{\odot}$ during the short-lasting Case BB RLO. This amount is a factor of ~ 4 smaller than what is needed to reach a recycled spin period of 30 ms according to Eq.(14) in Tauris et al. (2012). Hence, we can conclude that either PSR J2222–0137 accreted at a slightly super-Eddington rate (as also found for PSR J1952+2630 in Lazarus et al. 2014), or that the geometric factor $f(\alpha, \xi, \phi, \omega_c)$ introduced in Eq. (13) in Tauris et al. (2012) should be less than unity.

Whereas some MSPs must evidently have been inefficient accretors (e.g. Antoniadis et al. 2012), it has recently been argued that NS accretors in the ultraluminous X-ray binaries M82 X-2 (Bachetti et al. 2014) and ULX-1 in NGC 5907 (Israel et al. 2016) may even accrete at a rate of up to 100 times the Eddington limit to explain the observed X-ray luminosities of these sources ($L_X \sim 10^{40} \text{ erg s}^{-1}$) and the high spin-up rate of the latter NS. However, these sources are suggested to harbor very strong B-field NSs and are most likely not representative of pulsars in general. Nevertheless, we conclude that observations of accreting NSs and recycled MSPs continue to challenge the details of physical models for the accretion of matter onto magnetized compact objects.

Regardless of the abovementioned uncertainty in the exact amount of material accreted by PSR J2222–0137, the total amount of matter accreted was probably at most a factor of a

few $10^{-3} M_{\odot}$, or less than $10^{-2} M_{\odot}$ including wind accretion prior to the onset of RLO/CE of the IMXB progenitor system. Hence, the NS birth mass of PSR J2222–0137 was almost identical to the presently measured mass of $1.76 \pm 0.06 M_{\odot}$. This is the largest birth mass inferred for any radio pulsar. Of the other known $2 M_{\odot}$ pulsars, J0348+0432 could (but need not) potentially have accreted several $0.10 M_{\odot}$ (Antoniadis et al. 2013), and PSR J1614–2230 was the previous record holder with a minimum estimated birth mass of about $1.7 M_{\odot}$ (Tauris et al. 2011; Lin et al. 2011). A few NSs in high-mass X-ray binaries are likely born with larger masses (e.g. Tauris et al. 2017).

A NS birth mass of close to $2 M_{\odot}$ may, from a stellar evolution point of view, suggest a relatively massive progenitor star of at least $20 M_{\odot}$ (see discussions in Tauris et al. 2011, and references therein), although many aspects of the final outcomes of massive star evolution are still uncertain (Langer 2012). More importantly, such large NS birth masses are not easily obtained from current SN explosion modelling (Uglio et al. 2012; Pejcha & Thompson 2015; Ertl et al. 2016; Sukhbold et al. 2016) – even when fallback is included in 1D simulations. We notice that the parametrized modelling of Müller et al. (2016) results in some NSs with masses up to $2 M_{\odot}$. Interestingly enough, they originate from progenitor stars with initial ZAMS masses of only $\sim 15 \pm 1 M_{\odot}$, while less massive NSs (as well as black holes) are produced for initial progenitor star masses up to $\sim 27 M_{\odot}$. The lack of massive NSs from more massive progenitor stars ($20\text{--}25 M_{\odot}$) in the work of Müller et al. (2016) is possibly caused by their assumed maximum possible NS mass of $2.05 M_{\odot}$. Their results depend on the amount of accretion after shock revival and need to be confirmed by 3D modelling. Furthermore, it is possible that magnetohydrodynamic effects could still allow for explosions in cases where the neutrino-driven mechanism fails (H.-T. Janka, 2017, priv. comm.). Finally, it should be noted that above-mentioned SN simulations are based on different sets of progenitor stars, e.g. evolved with different wind-mass loss assumptions, and only considered explosions of isolated (i.e. non-stripped) stars.

Although the birth mass of PSR J2222–0137 is relatively large compared to that of other radio pulsars, it is still in accordance with, although a bit on the high side of, the NS birth mass spectrum of current SN modelling (see the results in Uglio et al. 2012; Pejcha & Thompson 2015; Ertl et al. 2016; Sukhbold et al. 2016; Müller et al. 2016).

7. CONCLUSIONS

In this work we present the results of four years of timing of PSR J2222–0137. The parallax we measure matches the VLBI parallax well within 1σ , this is encouraging since this quantity is especially sensitive to systematic effects in the timing. The proper motions match as well, but not so

closely. We find a significant and very robust offset of our timing position and the VLBI position, which we have investigated in detail. This offset is not caused by DM variations caused by the Sun or otherwise, and it does not change for different choices of Solar System ephemeris. Based on recent VLBI studies, we conclude that the uncertainty of the absolute VLBI position measurement for PSR J2222–0137 was likely under-estimated; however, it is also not clear whether this is the explanation for the observed offset.

We have obtained masses for both PSR J2222–0137 and its companion that are significantly larger than the masses presented in Paper I. The reasons for this are not entirely clear, but we believe our results to be more accurate because a) we have a larger number of observations and much improved orbital coverage and a larger baseline, b) we measure the rate of advance of periastron $\dot{\omega}$ with high significance, and (assuming GR) the observed value is in strong disagreement with the lower mass values presented in Paper I, but in a marginal agreement with ours. We conclude therefore that the measurement presented here is more accurate. This is corroborated by the observation in Paper I that the mass values from Shapiro delay change significantly when they fit for $\dot{\omega}$, indicating a correlation between these parameters. The highly significant measurement of $\dot{\omega}$ presented in this work is therefore important to reduce parameter correlations and allow the determination of accurate masses. Furthermore, based on the measurement of Ω presented in Paper I, we were able to determine the inclination of the system from the measurement of \dot{x} . Continued timing will achieve a high precision measurement of the component masses and inclination because the uncertainties in the measurement of $\dot{\omega}$ and \dot{x} decrease with the timing baseline T as $T^{-3/2}$.

The mass measurement for PSR J2222–0137 and the precise knowledge of its distance make its system interesting for tests of gravity theories, in particular for alternatives to GR that violate the strong equivalence principle and predict the existence of dipolar gravitational waves. The mass of PSR J2222–0137 falls into a range that so far is poorly constrained in terms of phenomena like spontaneous scalarization (Shao & Wex 2016), and for this reason makes an important contribution in testing scalar-tensor theories of gravity. Among others, this is important for future gravitational wave observations with ground-based gravitational wave detectors, like LIGO and Virgo (Shao et al. 2017).

The improved mass measurements are also important for understanding the evolution of the system. With a mass

of $1.293 \pm 0.025 M_{\odot}$; the companion of PSR J2222–0137 is one of the most massive WD companions to any pulsar known (e.g., Özel & Freire 2016). Such a massive WD is expected to crystalize and reach surface temperatures below 3000 K on a total timescale of 3 to 4 Gyr, explaining the non-detection of this WD in the most sensitive optical observations made to date. Detecting this WD with more sensitive optical observations, measuring its color and estimating its radius represent high priority goals.

Furthermore, given the relatively short timescale for the evolution of the progenitor star of the WD, the accretion episode could not have been long, and the total amount of mass transferred was likely $< 10^{-2} M_{\odot}$. Therefore this pulsar was born with a mass that was similar to its current mass, making it the largest NS birth mass measured to date for any radio pulsar. This measurement shows, furthermore, that the pulsars in IMBPs also have a wide range of masses: from $1.24 \pm 0.11 M_{\odot}$ for PSR J1802–2124 to $1.76 \pm 0.06 M_{\odot}$ for PSR J2222–0137 and even $1.928 \pm 0.017 M_{\odot}$ if we include PSR J1614–2230 in this class (Fonseca et al. 2016).

The mass measurement presented in this work plus those of PSRs J1614–2230 (Fonseca et al. 2016), J0348+0432 (Antoniadis et al. 2013), J1903+0327 (Freire et al. 2011) and J1946+3417 (Barr et al. 2017) show that massive NSs are not rare in the Universe. This becomes even clearer if we take into account the fact that we find this NS in one of the two known binary pulsars with measured masses within 300 pc of the Earth.

We thank Thomas Janka for discussions on NS birth masses, Adam Deller for discussions on the VLBI astrometry and Alessandro Ridolfi and John Antoniadis for proofreading and useful suggestions. The Nançay Radio Observatory is operated by the Paris Observatory, associated with the French Centre National de la Recherche Scientifique (CNRS). We acknowledge financial support from “Programme National de Cosmologie and Galaxies” (PNCG) of CNRS/INSU, France. PCCF gratefully acknowledges financial support by the European Research Council for the ERC Starting grant BEACON under contract No. 279702 during most of his work on this project. MK and GD acknowledge the financial support by the European Research Council for the ERC Synergy Grant BlackHoleCam under contract no. 610058.

Facilities: Effelsberg 100-m Radio Telescope, Nançay Radio Telescope, Lovell 76-m radio telescope

Software: Numpy, PSRCHIVE, tempo

REFERENCES

Antoniadis, J., Tauris, T. M., Özel, F., et al. 2017, ArXiv e-prints, [arXiv:1605.01665 \[astro-ph.HE\]](https://arxiv.org/abs/1605.01665)

Antoniadis, J., van Kerkwijk, M. H., Koester, D., et al. 2012, *MNRAS*, 423, 3316

- Antoniadis, J., Freire, P. C. C., Wex, N., et al. 2013, *Science*, **340**, 448
- Arzoumanian, Z., Joshi, K., Rasio, F. A., & Thorsett, S. E. 1996, in *Astronomical Society of the Pacific Conference Series*, Vol. 105, IAU Colloq. 160: Pulsars: Problems and Progress, ed. S. Johnston, M. A. Walker, & M. Bailes, 525
- Arzoumanian, Z., Brazier, A., Burke-Spolaor, S., et al. 2015, *ApJ*, **813**, 65
- Bachetti, M., Harrison, F. A., Walton, D. J., et al. 2014, *Nature*, **514**, 202
- Barr, E. D., Freire, P. C. C., Kramer, M., et al. 2017, *MNRAS*, **465**, 1711
- Bergeron, P., Wesemael, F., Dufour, P., et al. 2011, *ApJ*, **737**, 28
- Bertotti, B., Iess, L., & Tortora, P. 2003, *Nature*, **425**, 374
- Boyles, J., Lynch, R. S., Ransom, S. M., et al. 2013, *ApJ*, **763**, 80
- Camilo, F. 1996, in *Astronomical Society of the Pacific Conference Series*, Vol. 105, IAU Colloq. 160: Pulsars: Problems and Progress, ed. S. Johnston, M. A. Walker, & M. Bailes, 539
- Cordes, J. M., & Lazio, T. J. W. 2002, *ArXiv Astrophysics e-prints*, [astro-ph/0207156](#)
- Damour, T., & Deruelle, N. 1985, *Ann. Inst. Henri Poincaré Phys. Théor.*, Vol. 43, No. 1, p. 107 - 132, 43, 107
- . 1986, *Ann. Inst. Henri Poincaré Phys. Théor.*, Vol. 44, No. 3, p. 263 - 292, 44, 263
- Damour, T., & Esposito-Farèse, G. 1992, *Classical and Quantum Gravity*, **9**, 2093
- . 1993, *Physical Review Letters*, **70**, 2220
- . 1996, *Physical Review D*, **54**, 1474
- Damour, T., & Taylor, J. H. 1991, *ApJ*, **366**, 501
- Deller, A. T., Boyles, J., Lorimer, D. R., et al. 2013, *ApJ*, **770**, 145
- Deller, A. T., Vigeland, S. J., Kaplan, D. L., et al. 2016, *ApJ*, **828**, 8
- Demorest, P. B., Ferdman, R. D., Gonzalez, M. E., et al. 2013, *ApJ*, **762**, 94
- Deneva, J. S., Stovall, K., McLaughlin, M. A., et al. 2013, *ApJ*, **775**, 51
- Desvignes, G., Caballero, R. N., Lentati, L., et al. 2016, *MNRAS*, **458**, 3341
- Dewi, J. D. M., Pols, O. R., Savonije, G. J., & van den Heuvel, E. P. J. 2002, *MNRAS*, **331**, 1027
- Edwards, R. T., Hobbs, G. B., & Manchester, R. N. 2006, *MNRAS*, **372**, 1549
- Ertl, T., Janka, H.-T., Woosley, S. E., Sukhbold, T., & Ugliano, M. 2016, *ApJ*, **818**, 124
- Ferdman, R. D., Stairs, I. H., Kramer, M., et al. 2010, *ApJ*, **711**, 764
- Folkner, W. M., Williams, J. G., Boggs, D. H., Park, R. S., & Kuchynka, P. 2014, *Interplanetary Network Progress Report*, 196, 1
- Fonseca, E., Pennucci, T. T., Ellis, J. A., et al. 2016, *ApJ*, **832**, 167
- Freire, P. C. C., & Wex, N. 2010, *MNRAS*, **409**, 199
- Freire, P. C. C., Bassa, C. G., Wex, N., et al. 2011, *MNRAS*, **412**, 2763
- Freire, P. C. C., Wex, N., Esposito-Farèse, G., et al. 2012, *MNRAS*, **423**, 3328
- Gonzalez, M. E., Stairs, I. H., Ferdman, R. D., et al. 2011, *ApJ*, **743**, 102
- Habets, G. M. H. J. 1986, *A&A*, **165**, 95
- Hobbs, G. B., Edwards, R. T., & Manchester, R. N. 2006, *MNRAS*, **369**, 655
- Hotan, A. W., van Straten, W., & Manchester, R. N. 2004, "Proceedings of the Astronomical Society of Australia", **21**, 302
- Israel, G. L., Belfiore, A., Stella, L., et al. 2016, *ArXiv e-prints*, [arXiv:1609.07375 \[astro-ph.HE\]](#)
- Ivanova, N., Belczynski, K., Kalogera, V., Rasio, F. A., & Taam, R. E. 2003, *ApJ*, **592**, 475
- Ivanova, N., Justham, S., Chen, X., et al. 2013, *A&A Rv*, **21**, 59
- Kaplan, D. L., Boyles, J., Dunlap, B. H., et al. 2014, *ApJ*, **789**, 119
- Kopeikin, S. M. 1996, *ApJL*, **467**, L93
- Langer, N. 2012, *ARA&A*, **50**, 107
- Lazarus, P., Karuppusamy, R., Graikou, E., et al. 2016, *MNRAS*, **458**, 868
- Lazarus, P., Tauris, T. M., Knispel, B., et al. 2014, *MNRAS*, **437**, 1485
- Lin, J., Rappaport, S., Podsiadlowski, P., et al. 2011, *ApJ*, **732**, 70
- Liu, K., Desvignes, G., Cognard, I., et al. 2014, *MNRAS*, **443**, 3752
- Lorimer, D. R., & Kramer, M. 2004, *Handbook of Pulsar Astronomy*, Cambridge University Press, Cambridge, UK.
- Lynch, R. S., Freire, P. C. C., Ransom, S. M., & Jacoby, B. A. 2012, *ApJ*, **745**, 109
- Martinez, J. G., Stovall, K., Freire, P. C. C., et al. 2015, *ApJ*, **812**, 143
- Müller, B., Heger, A., Liptai, D., & Cameron, J. B. 2016, *MNRAS*, **460**, 742
- Özel, F., & Freire, P. 2016, *ARA&A*, **54**, 401
- Özel, F., Psaltis, D., Narayan, R., & Santos Villarreal, A. 2012, *ApJ*, **757**, 55
- Pejcha, O., & Thompson, T. A. 2015, *ApJ*, **801**, 90
- Radhakrishnan, V., & Cooke, D. J. 1969, *Astrophys. Lett.*, **3**, 225
- Rankin, J. M. 1983, *ApJ*, **274**, 333
- Reardon, D. J., Hobbs, G., Coles, W., et al. 2016, *MNRAS*, **455**, 1751
- Reid, M. J., Menten, K. M., Brunthaler, A., et al. 2014, *ApJ*, **783**, 130
- Robertson, H. P. 1938, *The Annals of Mathematics*, **39**, 101
- Shao, L., Sennett, N., Buonanno, A., Kramer, M., & Wex, N. 2017, *ArXiv e-prints*, [arXiv:1704.07561 \[gr-qc\]](#)
- Shao, L., & Wex, N. 2016, *SCPMA*, **699501**, 23
- Shao, L., Stairs, I., Antoniadis, J., et al. 2015, *Advancing Astrophysics with the Square Kilometre Array (AASKA14)*, 42

- Shibata, M., Taniguchi, K., Okawa, H., & Buonanno, A. 2014, *Physical Review D*, 89, 084005
- Shklovskii, I. S. 1970, *Soviet Ast.*, 13, 562
- Smits, R., Lorimer, D. R., Kramer, M., et al. 2009, *A&A*, 505, 919
- Sokolovsky, K. V., Kovalev, Y. Y., Pushkarev, A. B., & Lobanov, A. P. 2011, *A&A*, 532, A38
- Splaver, E. M., Nice, D. J., Arzoumanian, Z., et al. 2002, *ApJ*, 581, 509
- Sukhbold, T., Ertl, T., Woosley, S. E., Brown, J. M., & Janka, H.-T. 2016, *ApJ*, 821, 38
- Tauris, T. M., Langer, N., & Kramer, M. 2011, *MNRAS*, 416, 2130
- , 2012, *MNRAS*, 425, 1601
- Tauris, T. M., Langer, N., & Podsiadlowski, P. 2015, *MNRAS*, 451, 2123
- Tauris, T. M., Kramer, M., Freire, P. C. C., et al. 2017, ArXiv e-prints, [arXiv:1706.09438 \[astro-ph.HE\]](https://arxiv.org/abs/1706.09438)
- Taylor, J. H. 1992, *Royal Society of London Philosophical Transactions Series A*, 341, 117
- Taylor, J. H., & Weisberg, J. M. 1982, *ApJ*, 253, 908
- Ugliano, M., Janka, H.-T., Marek, A., & Arcones, A. 2012, *ApJ*, 757, 69
- van Straten, W., Demorest, P., & Osłowski, S. 2012, *Astronomical Research and Technology*, 9, 237
- Will, C. M. 2014, *Living Reviews in Relativity*, 17, 4
- Xilouris, K. M., Kramer, M., Jessner, A., et al. 1998, *ApJ*, 501, 286